Journal of Hazardous Materials Advances 14 (2024) 100433

Contents lists available at ScienceDirect

Journal of Hazardous Materials Advances

journal homepage: www.elsevier.com/locate/hazadv

Experimental investigation of the fallout dynamics of microplastic fragments in wind tunnel: The BURNIA agenda

Matteo M. Musso [a,d], Frank Harms [b], Massimo Martina [a], Elke K. Fischer [c], Bernd Leitl [b], Silvia Trini Castelli [d,*]

[a] Department of Physics, University of Torino, Torino, Italy
[b] Meteorological Institute, University of Hamburg, Hamburg, Germany
[c] Institute of Geography, University of Hamburg, Hamburg, Germany
[d] Institute of Atmospheric Sciences and Climate, National Research Council, Torino, Italy

ARTICLE INFO

Keywords:
Atmospheric microplastics
Settling velocities
Wind-tunnel experiments
Stokes law
Empirical approaches

ABSTRACT

We present a methodology and the first tests to estimate the settling velocity of airborne microplastics based on wind tunnel experiments. A novel approach and original perspective are proposed, discussing in detail challenges and faced problems, both on the theoretical and experimental sides. Several experiments were performed, releasing fragments of different microplastic types, PET, PVC and LPDE. A statistical analysis was applied to the measurements and the values of the settling velocities were estimated to range between 0.1 and 0.2 ms^{-1}, in agreement with most values found in the related literature. Based on the observed velocities, the applicability of the Stokes' law, which is often used also for airborne microplastics, is then addressed, highlighting its potential limitations in the context of the microplastic dynamics in the atmosphere. We confirm that using the Stokes' law may lead to a substantial overestimation of the settling velocity for the airborne microplastics. We also recommend to consider moving to the concept of 'effective deposition velocity', to account for the turbulent processes characterising the real atmosphere.

1. Introduction

Microplastic (MP) particles, defined as particles consisting of synthetic polymers with a size in the range $s \simeq 1$ μm–5 mm, are ubiquitous in our environments (Arthur et al., 2009). They originate from various sources and are defined according to their generation as either being primary or secondary MPs. Primary MPs are generated on purpose in this specific dimension (e.g. production pellets, microbeads and abrasive particles) whereas secondary MPs derive from degradation mainly induced by UV radiation or physical breakdown and abrasion (Andrady, 2011). The term microplastics integrates particles with different characteristics according to particle size, morphology (e.g. fragments, filaments/fibres, spheres, films) and chemical composition (e.g. polyethylene, polystyrene, polyamide, polyethylene terephthalate). The latter largely determines the material density of the particle, which is, however, further modified by e.g. ageing and the use of additives (Hartmann et al., 2019). Research very much focused on marine ecosystems but also covered terrestrial ecosystems and the related multiple sources such as industrial or agricultural applications, landfills, littering and construction (Xu et al., 2020; Rochman, 2018). Major pathways have been identified to be large rivers, and, in recent years atmospheric transport of MPs (Zhang et al., 2020; Schmidt et al., 2017). MPs in the atmosphere have been shown to be most present in urban surroundings and thus being especially prone to human exposure (Klein et al., 2023; O'Brien et al., 2023; Li et al., 2020; Cai et al., 2017). Several studies have highlighted the presence of MPs deposited in protected areas (Brahney et al., 2020) and remote regions, such as French Pyrenees (Allen et al., 2019), Tibetan Plateau glaciers (Zhang et al., 2021), Arctic (Bergmann et al., 2022), Antarctic (Aves et al., 2022) and European Alps (Parolini et al., 2021; Ambrosini et al., 2019), and in the Oceans (Allen et al., 2022; Trainic et al., 2020; Wang et al., 2020; Allen et al., 2020; Liu et al., 2019), drawing the attention to the key role of the atmospheric transport in explaining the presence of MPs far away from any significant source.

A variety of plastic particles are released into the environment and are subjected to transformation and degradation processes. Thus a fairly wide range of sizes can be expected to characterise the airborne MPs. The study of the complex processes that drive the dispersion of MPs in the air, including the atmospheric turbulent motions, the various deposition and resuspension processes and the effects of the radiation, is still pioneering. In this context, a number of aspects need further

* Corresponding author.
E-mail address: s.trinicastelli@isac.cnr.it (S. Trini Castelli).

https://doi.org/10.1016/j.hazadv.2024.100433
Received 26 March 2024; Received in revised form 10 May 2024; Accepted 12 May 2024
Available online 17 May 2024

investigation, to understand how effective the atmosphere is as a carrier of MPs, what is its contribution to the fallout on water and soil and at which spatial and temporal scales relevant airborne transport and deposition take place. In particular, it has to be understood what are the relative contributions of different processes on the MP transport and deposition. These are gravitational settling and dry deposition, re-suspension and transport in saltation mode, namely the grass-hopper effect, turbulent transport and mixing, capture and comb-effect by surface roughness elements and vegetation, and wet scavenging by washout and rainout. In addition, the type of material, the MP structure and morphology and its lifetime can be expected to interfere with such processes and to affect their effectiveness. The estimation of the average time a plastic particle spends in the atmosphere is fundamental for investigating the crucial role played by the atmospheric transport concerning the spread of MPs.

An important parameter is the value of the MP settling velocity, v_s, defined as the terminal velocity reached by a particle moving in a still fluid due to gravitational forces. The time a MP particle may spend in the air is directly correlated to its settling velocity. This parameter is evaluated via the balance between the external forces F_e, such as gravity and buoyancy, driving the vertical motion of the particle in the fluid, and the drag force F_d, affecting the particles depending on its motion in the fluid. In general, the drag force depends on a range of parameters characterising the fluids and particles, such as particle size, shape and roundness, density, fluid viscosity, as well as the Reynolds number of flow around the particle. For this reason, there is not a general and universal equation providing the correct evaluation of v_s, in particular when considering odd-shaped particles, like MPs can be, not characterised by effective shape and drag. A simple and largely used formula is given by the Stokes' law (see Section 2), often used as a starting point for both experimental and theoretical work trying to provide empirical or theoretical formulations for v_s for different particles and fluid parameter (Baba and Komar, 1981). A few works have provided an estimation of the airborne MP settling velocity. Based on the study by Zender et al. (2003), Allen et al. (2019) estimated a value of $v_s = 0.1\ \mathrm{ms}^{-1}$ for a 25 μm size dust particle and used it as representative for MPs settling velocity in the numerical simulation supporting their experimental campaign in the French Pyrenees. Following Allen et al. (2019), Wright et al. (2020) used the Stokes' law to provide values of the settling velocity for both fibrous and non-fibrous MPs sampled during an experimental campaign in London, UK. The most frequent MP fragments were made of polystyrene (PS) with typical size $s \sim 100$ μm and density of $\rho = 1050\ \mathrm{kg\ m}^{-3}$, with an associated settling velocity estimated as $v_s \sim 0.32\ \mathrm{ms}^{-1}$. Concerning the fibres, the most common material was polyacrylonitrile (PAN), with a density of $\rho \sim 1184\ \mathrm{kg\ m}^{-3}$ and a typical length ($l \sim 400$ μm) to width ($d \sim 20$ μm) ratio $\beta \sim 20$. These led to calculating a settling velocity for the fibrous material of $v_s \sim 0.06\ \mathrm{ms}^{-1}$. Trainic et al. (2020) estimated the settling velocity for airborne MPs following the theory for the measurements of terminal velocities for water droplet and ice needles with size in the range of $s \sim 10-100$ μm (Westbrook, 2008). Since the shape, size and density of the MPs they analysed were close to this range, they were able to provide resulting values of settling velocities in the range $v_s \sim 0.001$–$0.2\ \mathrm{ms}^{-1}$. All previous approaches provided consistent results, at the same time reporting the approximations that had to be assumed, like referring to dust particles as representative material for MPs (Allen et al., 2019), using theories that apply to droplets and crystals (Trainic et al., 2020) or considering a fragment size (Wright et al., 2020) that might exceed the range of confidence for the Stokes' law. In particular, Zender et al. (2003) estimated that the Stokes velocity overestimates sedimentation by more than 10% for $s \gtrsim 20$ μm. These limitations highlight that an established methodology to measure or estimate the settling velocities for the various airborne MPs is still missing, underlining the need to set up additional investigation considering the specific conditions of the MP transport in the air (particle-wise as well as flow-wise), even supported by dedicated experimental programs.

An advantageous approach is to conduct experiments in wind-tunnel facilities, which enable studying the settling and transport behaviour in both still and turbulent air flows, similar to full-scale conditions. The number of laboratory experiments aimed at studying the aerodynamic behaviour of MPs is small, and among them a few were carried out in wind-tunnel facilities, yet focusing mainly on the effectiveness of wind erosion on MPs from the soil and their potential entrainment in the air. Rezaei et al. (2019) investigated the impact of wind erosion on the terrestrial transport of MPs. The experiments were conducted for different soils in the Iranian desert, by simulating the wind erosion effect with the use of a portable wind tunnel. The comparison between the MPs enrichment in the original soil and the one of wind-eroded sediments, highlighted a higher presence of MPs in the latter case. This result underlines the importance of the wind erosion effect for the transport of airborne MPs toward terrestrial locations and for their exchange between the soil and the atmosphere. Bullard et al. (2021) investigated the effectiveness of wind in mobilising MP particles and the impact of wind erosion over different soil types on the air entrainment of MPs of different morphologies, beads and fibres. This was performed by mixing different substrates with various concentrations of MPs and analysing the enrichment ratio (i.e. the ratio between the MPs content in the observed flux and the one of the substrate) downwind at various distances from the source. Their results showed that the presence of MPs did not lead to a significant contribution to wind erosion thresholds. Yet, the particle flux increased when substrates subjected to wind erosion were mixed with plastic material. The authors suggested that, since the enrichment ratio did not vary significantly within 2-m distances downwind of the source, particles may be transported away from it once entrained into the air.

We consider that wind tunnel experiments have the potential to play a fundamental role in the understanding of the physical processes specifically determining the airborne transport of MPs and the interaction with the ground. They can contribute in studying the processes in controlled conditions, thus addressing the related unknown parameters that can be difficult to investigate based only on field measurements. We refer, for instance, to (i) the settling and deposition velocity of different types of MPs in turbulent flows and related deposition effect, (ii) the potential of the entrainment and of the deposition and accumulation processes, (iii) the effect of the dimension and morphology for the different types of MPs on their airborne transport, (iv) the specific dynamics of the airborne trajectories for the different types of MPs, (v) the effectiveness of re-suspension, saltation and creep-mode processes for secondary transport and dispersion. In this work, we present an approach that can be complementary to field experiments, to set the ground for studying the specific aerodynamic properties of the MPs. As a first step, exploratory experiments aimed at estimating the effective settling velocity for different samples of plastic particles were carried out in the Environmental Wind Tunnel Laboratory (EWTL, https://www.mi.uni-hamburg.de/en/arbeitsgruppen/windkanallabor.html) of the Meteorological Institute of Hamburg University, in the frame of the BURNIA collaboration (BUrst-in Research in a Niche International Ambient). The experiments were conducted in the small boundary layer wind tunnel facility "BLASIUS" in the EWTL. The wind tunnel was chosen to provide a confined space for initially measuring settling velocities under no wind conditions but with the possibility to investigate transport behaviour under wind flow conditions similar to those in the atmospheric boundary layer. Particularly for irregularly shaped MPs, trajectory and transport behaviour are expected to differ from that under idealised settling conditions without moving air. In our perspective, one main goal is to establish the framework for seeking reliable and efficient methodologies to investigate the airborne properties of the MPs. Specifically, here we are interested in discussing the potential feasibility of conducting these types of experiments, addressing the approximations we had to deal with, and the limitations and problems we encountered. This kind of analysis and connected information are seldom discussed in detail, and we retain it

useful to share them. We notice that building a proper experimental framework is the pathway to estimate quantities that are needed by numerical models to study and assess the MP dispersion, distribution and environmental impact at all scales, from local to global.

To discuss the applicability of Stokes' law for airborne MPs, the theoretical equations for the definition and calculation of the settling velocity are reported and described in Section 2. The experimental setup as well as the specific goals of the measurement approach and related challenges are illustrated in Section 3. The observations are analysed and results are discussed in Section 4 and in Section 5 conclusions and possible future developments are drawn.

2. The role of Stokes' law as theoretical model

Although experimental evidence has validated the Stokes' law for settling velocity both for spherical particles and fibres (based on the equivalent diameter) of different material (Henn, 1996), its applicability to atmospheric MP deposition processes has not yet been sufficiently demonstrated and proved experimentally. Particularly for non-spherical particles in flows with extremely varying turbulence characteristics, Stokes' concept might be considered as too simplifying. The measurements carried out in the wind tunnel can provide data to be used for comparison with the theoretical values, addressing the feasibility of using the Stokes' law for the airborne MP. Hereafter we recall the main formulations.

The settling velocity characterising the relative motion of a spherical particle in a static incompressible viscous Stokes fluid, is given by the balance between the gravitational, buoyancy and drag forces, which are:

$$\begin{cases} F_g &= (\rho_p - \rho_f) g V, \\ F_d &= 3\pi\mu\ d v. \end{cases} \tag{1}$$

written in terms of the particle and fluid densities ρ_p, ρ_f, the gravitational acceleration g, the particle volume $V = \frac{1}{6}\pi d^3$, the dynamic viscosity μ, the particle velocity v and its spherical diameter d. When the two forces are equal, the Stokes settling velocity v_{Stokes} is retrieved by solving for the particle velocity v:

$$v_{Stokes} = \frac{g d^2 (\rho_p - \rho_f)}{18\mu}. \tag{2}$$

The Stokes' law is a good approximation for the settling velocity of spherical particles in low Reynolds number condition, $Re \lesssim 0.1$. It is a common understanding to consider that Stokes law can be applied to particles whose diameter size ranges as $d \simeq$ 1–80 μm: larger with respect to fluid molecules, not to be affected by their Brownian motion, and small enough not to reach high settling velocities that may trigger turbulence in the fluid. Although this equation holds for spherical particles, several works were published trying to take into account all parameters that may affect the Stokes settling velocity such as shape, roundness etc. (see e.g. Dietrich, 1982) and several semi-empirical correction factors were derived. Experiments aiming to investigate the settling velocity of different particles focused mainly on the dependency of the drag coefficient C_D as a function of the Reynolds number Re, in order to drop the Stokes approximation of steady, viscous flow. On the other hand, though, dropping the spherical approximation is a difficult challenge. For this reason, several correcting factors based on the different shapes, sizes and roundness have been historically derived to treat also non-spherical particles. The K correction factor for ellipsoidal particles (McNown and Malaika, 1950) or the shape factor for naturally shaped particles (Janke, 1966) are among the oldest proposed solutions. Among all the corrections, since MPs take also fibrous shapes, it is worth mentioning the correction factor to the Stokes' law for fibres, by assuming a cylindrical shape of the particles. The settling velocity does not change its formulation, except that the equivalent diameter D is used instead of the spherical one d (see Zender et al., 2003; Henn, 1996):

$$D = \frac{3 D_c}{2\sqrt{\frac{0.558}{\ln(2\beta) - 0.5} + \frac{1.788}{\ln(2\beta) + 0.5}}} \tag{3}$$

where D_c is the cylinder radius, i.e. the width of the fibre, and β is the aspect ratio of the length over width. In the derivation of Eq. (3), to account for the fact that the cylinder may change its orientation while settling, it is assumed that it tends to maximise also its drag. This behaviour is known as *preferential orientation*. If the aspect ratio of the fibre is $\beta \gtrsim 20$, Eq. (3) simplifies as:

$$D \approx D_c \sqrt{\ln(2\beta)}. \tag{4}$$

Similarly, Henn (1996) derived a formulation for the aerodynamic equivalent diameter D_a of a fibre, retaining the fibre density because the density terms do not cancel in its derivation. For a fibre with a length-to-width ratio $\beta \gtrsim 20$, the D_a results approximately:

$$D_a \approx D_c \sqrt{\rho_p \log(2\beta)}. \tag{5}$$

Notice that this is the formulation that was used by Wright et al. (2020) for the calculation of v_s for the fibrous plastic particles.

We recall that here we aim to investigate the feasibility of laboratory experiments to estimate the values of the settling velocity for plastic fragments and particles lying in the microplastic range, 1–1000 μm according to ISO/TR 21960:2020 (2020). A first simple setup for this investigation has been arranged, as detailed in Section 3. When preparing the experimental setup, particular care has to be taken in determining the time interval that a particle takes during its fall to reach its terminal velocity, thus defining its settling value. We proceeded as follows.

Based on Eq. (1), the total force acting on a particle falling in the air, neglecting the contribution of the air density ρ_f that is much smaller than the MP material, is given by the sum of gravity and drag:

$$m \frac{d v(t)}{dt} = mg - b v(t) \tag{6}$$

where m is the mass and b is a drag force coefficient, here assumed constant in time and depending only on particle parameters. A simple way to solve Eq. (6) is to multiply both the right and left hand sides of the equation by $\exp\left(\frac{b}{m}t\right)$, leading to:

$$\frac{d}{dt}\left[v(t) \exp\left(\frac{b}{m}t\right)\right] = \exp\left(\frac{b}{m}t\right) g \tag{7}$$

for which the solution is

$$v(t) = C_1 \exp\left(-\frac{b}{m}t\right) + \frac{mg}{b} \tag{8}$$

where C_1 is the integration constant. By using the initial condition $v(t = 0) = 0$ the equation reads:

$$v(t) = \frac{mg}{b}\left[1 - \exp\left(-\frac{b}{m}t\right)\right], \tag{9}$$

where $\frac{mg}{b} = v_f$ is the terminal velocity reached asymptotically by the particle and $\frac{m}{b} = \tau$ is the time scale.

The corresponding equation of motion for the particle is retrieved by integration since $v(t) = \frac{dz(t)}{dt}$, leading to:

$$z(t) = \frac{mg}{b}\left[t + \frac{m}{b}\exp\left(-\frac{b}{m}t\right)\right] + C_2, \tag{10}$$

where the integration constant is retrieved from the initial condition $z(0) = h$. In this way $C_2 = h - \frac{gm^2}{b^2}$, leading to:

$$z(t) = h + \frac{mg}{b}\left[t + \frac{m}{b}\exp\left(-\frac{b}{m}t\right) - \frac{m}{b}\right] \tag{11}$$

Finally, Eqs. (9) and (11) are rewritten as:

$$\begin{cases} v(t) &= v_f\left[1 - \exp\left(-\frac{t}{\tau}\right)\right] \\ \Delta z(t) &= v_f\left[t + \tau\exp\left(-\frac{t}{\tau}\right) - \tau\right] \end{cases} \tag{12}$$

where $\Delta z(t)$ is the vertical distance covered by the particle falling from a height h to the height $z(t)$ in the time t. From the velocity profile, it can be shown that, after a time $t \sim \tau, 2\tau, 3\tau$ a particle reaches a velocity $v \sim 0.63v_f, 0.85v_f, 0.95v_f$ respectively. Thus we can consider that the settling velocity is reached by particle after a time $t \simeq 3\tau$.

3. The BURNIA experimental setup

The BURNIA experiments were carried out in the BLASIUS wind tunnel, which consists of a 10 m long test section with a cross section of 1.5 m × 1 m and provides means for controlled turbulent flows and simulating atmospheric boundary layer flows at reduced scales. Mean wind speed can be precisely controlled from 0 ms^{-1} to approximately 10 ms^{-1}. The wind tunnel is designed as closed test section – open return wind tunnel facility operated in suction mode. As common for boundary layer wind tunnel facilities, the test section is equipped with a height adjustable ceiling for precise control of momentum fluxes in simulated atmospheric boundary layer flows, ensuring turbulence characteristics similar to full-scale conditions. Laboratory grade visualisation and measurement equipment such as Laser Doppler anemometry or particle image velocimetry can be used for accurate, non-intrusive and turbulence-resolving flow measurements.

3.1. The microplastic samples

The tested MP sample consisted of four different plastic materials, polyvinylchloride (PVC), polyethylene terephthalate (PET), low-density polyethylene (LDPE) and polypropylene (PP), of different sizes and shapes. The results discussed in Section 4 refer to the fragment-shaped particles (PVC, PET, LDPE) while, due to experimental challenges and difficulties, tests with fibrous material are not supported with quantitative results (see Section 3.3) and require further investigation. Table 1 reports the characteristics of the different samples. The density and nominal size of the reference polymer particles refer to indications provided by the supplier (Goodfellow Cambridge Ltd). For the PET, a range of density was indicated and we chose a value within it by referring to literature (Rosato et al., 2004). The density of the particles in the PVC and PET samples is reported to be nearly the same, while the density of the LDPE particles is lower.

The reference materials used are provided in powder form. The particles contained do not have a fully rounded morphology but correspond to the morphology of fragments in the sense of irregularly shaped particles. This is consistent with the findings of a dominance of fragments in environmental samples compared to e.g. spheres and fibres and thus represents an approximation to real conditions (Burns and Boxall, 2018; Phuong et al., 2016). The reference particles were selected according to comparable nominal particle sizes, here equivalent to 250–300 μm, which according to our analyses tend to represent the largest size of the particles contained in the samples. Despite the specified nominal size, there appears to be a wide range of particle sizes contained in the sample material, as noticeable by the magnification in Fig. 1, thus the real size of the particles differs from the nominal one. Therefore, a microscope-based measurement of the size spectrum was performed (AxioScope 5/7 KMAT, automated image analysis via Zeiss Zen 3.0, Intellisis). The resulting statistics are reported in Table 1, highlighting that the maximum size is the one approaching the nominal value. The heterogeneity of the particle sizes in the sample materials has thus to be considered when discussing the results of the measurements.

There are methods to further select the particles in the sample, in order to narrow the distribution of their sizes. The particles are subjected to wet sieving to generate a target size spectrum. During this wet sieving, larger and smaller adhering particles are excluded. However, further separation of particles by wet sieving them was not considered in this study in order to avoid possible aggregation, complicating their use in wind tunnel tests. Non-standard, irregular and rather wide size distributions containing differently shaped particles are expected to be more realistic with reference to conditions in the atmosphere. As an initial step, we kept the samples as they were, considering also that they are somehow representative of the mixture commonly found when collecting MPs in the real world. In the analysis, it was kept in mind that size and shape equally influence particle aerodynamics, transport behaviour and thus, settling velocity even for narrow size distributions of differently shaped MP particles.

3.2. The methodology in a jar: the particle release device

The plastic material was put into a cylindrical glass container with an inlet and an outlet at the top. Pressurised air was applied via the inlet, forming a turbulent swirling jet flow which is mixing with the MP particles in the container. This simplified “fluidized bed vaporiser” for solid particles provided an air stream mixed with particles which was released vertically upwards to dissipate vertical release momentum of the particles before they fell down while passing the measurement area below the release height. Fig. 2 reports a sketch of the experimental setup.

The mechanism for the release was devised to ensure a null initial vertical momentum, in order to properly follow the settling of the particles. For recording particle trajectories, a 3D particle tracking was not yet feasible. Instead, a thin vertical LASER light sheet was utilised to visualise the vertical component of trajectories of falling particles. The sheet of LASER light illuminated a subset of the cloud of particles, to allow recording precise fall trajectories with a conventional high quality picture camera. A DSLR camera (Nikon D5300, APS-C sensor) was used to capture the vertical component of trajectories. In order to minimise optical distortion, the camera was equipped with a calibrated high quality full-frame camera lens (Nikkor 85/1.8D). Different exposure settings were applied for recording in order to check for consistency and robustness of measurement results. Longer exposure times lead to longer particle tracks, reducing the uncertainty in image-based distance measurements but increase the risk of biased measurements due to possible out of plane motion. Discrete image snapshots were taken under quasi-stationary experimental conditions with particles being released continuously. For the recording of images, wind tunnel lights were switched off to increase the contrast of recorded trajectories. All the tests were performed in a zero-wind condition, as a starting point. An example for a trajectory pattern recorded in such a condition is shown in Fig. 3.

For subsequent velocity analysis, a rule located in the light sheet was recorded before capturing trajectories. This enabled lines of pixels to be translated into travel distances of particles for a given exposure duration. In each recording session, a series of pictures was taken in order to increase the number of recorded trajectories for a statistically safe analysis and robust estimation of settling velocities. Image processing and velocity analysis was automated via a Python™ (version 3.10.6) script, using its standard libraries and other non-standard libraries such as *cv2* package (Bradski, 2000) for image processing and automated analysis. The image analysis consisted of the following steps:

- colour/contrast/sharpness correction of the recorded images
- automated trajectory line detection, using *cv2.findCountours* and *imutils.grab_contours* functions
- translation of trajectory lengths in pixels in mm by means of the reference rule recording
- calculation of settling velocity per trajectory by dividing the trajectory length by the exposure duration
- post-processing of the ensemble of settling velocities by means of a noise reduction algorithm to detect and remove outliers
- plotting of histograms and calculation of statistical measures of the sampled velocity distributions

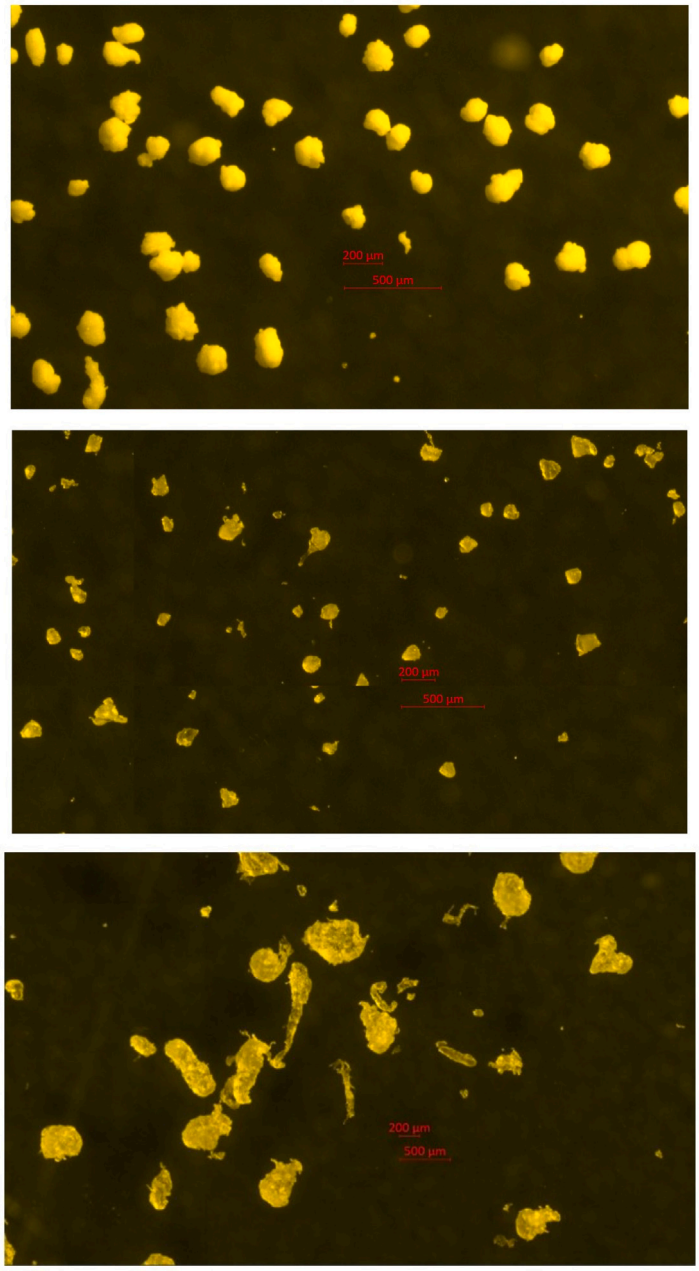

Fig. 1. Magnification of the picture of the samples of plastic particles for PVC (top), PET (centre) and LDPE (bottom) material.

Table 1
Nominal parameters of the plastic fragments for the different samples and statistical metrics related to their microscope-based measured sizes.

Material	Density ρ(kgm^{-3})	Nominal s (µm)	N. of MPs for statistics	Minimum s (µm)	Mean s (µm)	Median s (µm)	Maximum s (µm)	Std dev σ(µm)
PVC	1400	250	723	20	125	130	297	64
PET	1380	300	3293	21	95	86	290	46
LDPE	920	300	1408	19	41	31	271	30

In more detail, the length of the vertical component of each trace in pixel units was derived by analysing the pictures and the length l_{px} of one pixel in mm was estimated by comparison with the associated graduate scale of the ruler, as $l_{px} = \frac{\Delta s}{p}$, where Δs is the length in mm measured with the graduate scale, and p is the number of pixels in the picture corresponding to Δs. For example, in the case of Fig. 3, a $\Delta s =$ 164 mm, $p = 4008$, leading to $l_{px} = 4.1\ 10^{-4}$mm. An error of $\pm 0.4\ 10^{-4}$mm is associated with this estimate, by calculating it through the error propagation referring to the sensitivity of 1 mm of the measuring scale.

The traces were recorded when the particles had already reached their terminal velocity (see Section 3.3). For each trace, the relative particle settling velocity was computed as $v_s = \frac{l_{px} p_t}{\tau}$, where p_t is the number of pixels of the trace and τ is the exposition time of the camera, ranging between 0.0125 s and 0.02 s. The dataset of the particle

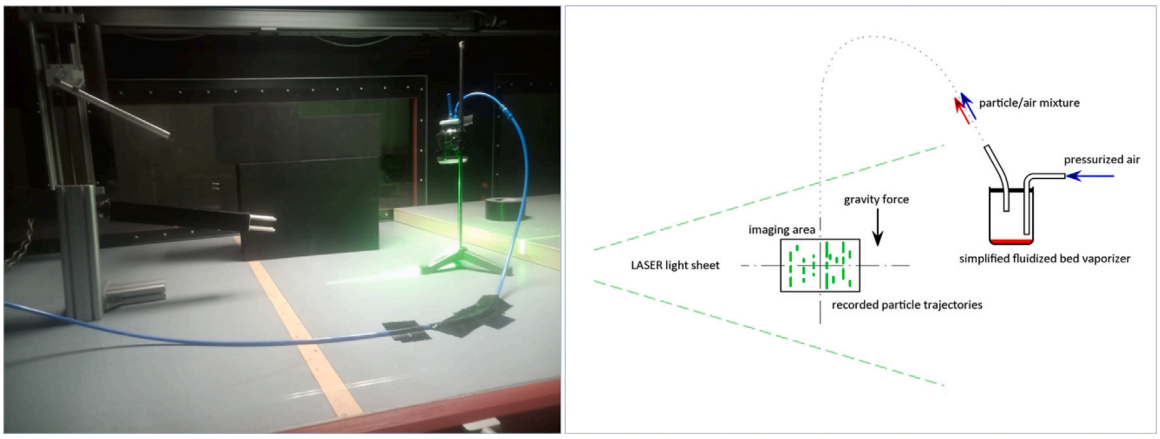

Fig. 2. Picture (left) and figurative sketch (right) of the experimental setup.

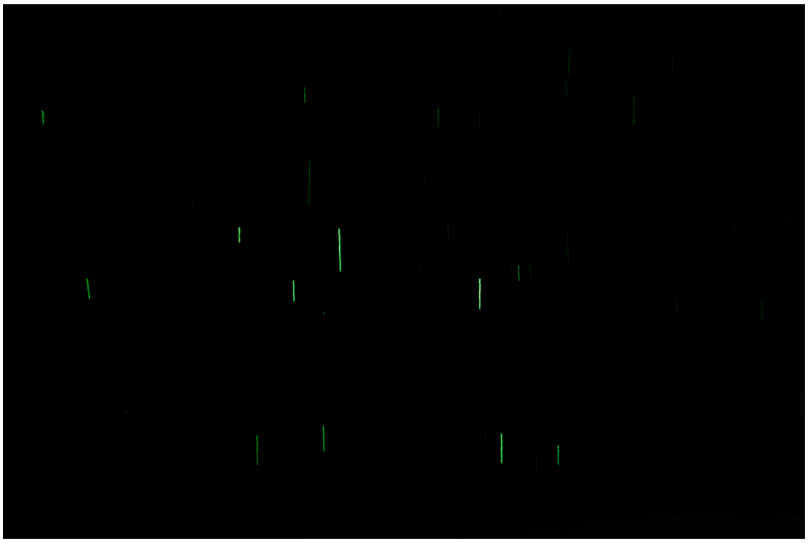

Fig. 3. Illustrative snapshot of the traces left by the falling MP particles.

velocities was elaborated based on noise reduction processes (see Section 4.1), and the average settling velocity $\langle v_s \rangle$ was calculated for each filtered sample, together with the corresponding standard deviation and median. To describe the distribution of the data histograms were produced.

3.3. The challenges

Since one of the goals here is to address the feasibility of straight forward experiments for estimating realistic particle settling velocities, in this section we present and discuss the problems encountered during experiments, in particular referring to uncertainties, and the complications that arose during the experiments, in particular referring to noise sources.

The theory in the air. A fundamental issue is the definition itself of the settling velocity, as the terminal velocity of a particle falling in a still fluid. From the theoretical viewpoint, considering as acting forces on a particle only the gravity, buoyancy and aerodynamic drag is a basic approximation that can be hardly satisfied in the real atmosphere. In particular, the atmosphere is intrinsically non-stationary but characterised by turbulent motions and diffusion. Since air hardly ever is absolutely at rest, this leads to the definition of an (effective) deposition velocity including not only the particle sink rate but also the effect of turbulent motions. Controlled experiments in qualified and dedicated wind tunnels are likely to be the framework that may best meet the theoretical requirements, making such an approximation acceptable. Even when considering air as a continuum, it is not trivial to create a volume of air being absolutely at rest. Otherwise, calm air is a precondition for measuring a true settling/sink rate of particles. In the test setup described above, slight movements of air in the closed test section of the wind tunnel are possible due to possible air motion in the laboratory room hosting the wind tunnel. For sure, the small but existing jet release of the MP/air mixture triggers slight movements of air, intended to be kept far enough away from the measurement section in the described setup.

The strict definition of 'settling velocity'. The definition of the settling velocity of a particle falling in a fluid implies the balance between the gravitational force and the drag force. When a particle with initial null momentum starts its fall, it will be accelerated by gravity for a certain time period before reaching its terminal constant velocity after such balance is achieved. Therefore, the setup of the release and of the detection area has to be arranged to ensure measuring the correct experimental quantity. In Section 2 we report a calculation that can be applied to make the experimental setup meet such requirements. We could verify that the measurements were taken after the particles achieved their terminal velocity, as follows. Assuming that the drag force for a viscous flow is proportional to the velocity, as in Eq. (6), and referring – to be conservative – to the measured settling velocity with the highest value for the 90th percentile filter (see Section 4 and Table 2), the time scale $\tau = v_f/g$ for the present experiments takes values

0.020, 0.024, 0.033 s for PVC, PET and LDPE respectively. Considering a time $t = 3\tau$, from Eq. (12) the distance within which the particle reaches the 95% of its terminal velocity is $\Delta z = 0.008,\ 0.012,\ 0.02$ m. In the wind tunnel, the particles had their initial vertical momentum equal to zero at about 1m height and the camera took pictures approximately ~ 0.9 m below, thus the observed velocity values are considered to be representative of their settling velocity.

Momentum-free particle release. To estimate the settling velocity of the particles during their fall, the projection of their trace in the vertical direction is measured. In principle, the initial momentum of the particle motion has to nullify, so that the remaining velocity of the particle is due only to the gravitational process. The setup for releasing MP particles necessarily leads to an initial momentum of particles at the point of their release. In order to efficiently dissipate the initial momentum, the air–particle mixture was released vertically upwards, causing the particles to rise until the vertical component of the release momentum was dissipated and particles started falling. Possible horizontal components of initial momentum were kept as small as possible but must be considered during the analysis and interpretation of results. When measuring deposition velocities of particles with ambient winds, the effect of wind components causing drag forces in all directions becomes substantial and has to be accounted for. At present, in the approach used for the computation, based on formulas in Eq. (1), the horizontal component, considered not substantial, is not included.

Vertical trajectory. A particle may keep having a horizontal velocity component v_{hor}, which can be longitudinal or transversal with respect to the laser sheet, thus crossing it in a diagonal direction. Transversal motion, causing particles to enter or leave the vertical light plane during exposure, will lead to shorter tracks in the recorded image, leading to an underestimation of settling velocity. The probability of particles leaving or entering the image plane can be lowered by using as short as reasonable exposure time. However, this approach will also result in a lower number of pixels forming a trajectory, thus increasing the relative uncertainty of track length measurements. Such a solution might be problematic also because too short traces, in particular when treating very small particles, might be hardly distinguished from traces left by any sources of noise, such as dust particles.

Traces fragmentation. The Python™ script relies on the different illumination of the traces on the snapshots with respect to the background, so as to consider as traces the appropriate portion of the image. When a trace is non-homogeneously illuminated, the algorithm for the analysis might interpret it as composed of different smaller traces, i.e. a single trace gets "fragmented" into smaller traces. This is a relevant source of uncertainties, since ensuring a homogeneous illumination for any particle is challenging for the nature of the experiment. The light plane is formed from a laser beam via a cylindrical lens. The intensity of light within the laser beam shows an almost Gaussian distribution with the maximum intensity at the centre of the beam. Hence, the light plane used for illuminating particles exhibits also a decay of light intensity in both, lateral and transversal directions. This may affect the length of recorded particle tracks if scattered light intensity is reaching the detection limit of the camera sensor. In order to minimise this effect for the particle motion, only the very central part of the light sheet is used as the area of imaging. Considering the possible decay of light intensity in the transversal direction, normal to the image plane, is a bit more challenging. For this reason, only the brightest recorded light tracks with almost no variation of light intensity along the track should be used for analysis. The loss in the number of useable tracks might be compensated by recording a larger number of individual images.

Wind Tunnel Dust. Another problem occurring during the experiments described here was that the wind tunnel is located and operated in a normal laboratory environment with regular cleaning, but not in a clean room. This means dust particles possibly being present in the recordings as well. For the particle material investigated so far, the trace length of the dust was much shorter than the average length for MPs, thus it was easy to distinguish between 'accidentally recorded environmental dust' and MP particles because of detectable differences in the corresponding settling velocities. The problem might become more relevant when working with smaller MP particles (i.e. plastic particles of the size $s \simeq$20–50 μm), and/or choosing lighter plastic material, for which the signal of the dust might be confused with that of the particles. The filtering approach introduced in next Section 4 could be used for dealing with this source of noise as well.

Handling fibres. In this work a first attempt was done to test the solidity of the setup to handle fibrous-shaped particles. Fibres were retrieved from a polypropylene (density $\rho = 900$ kg m^{-3}) bundle of strings and, as a preparatory test, were cut manually. For this reason, there was not a precise control on the regular length of each fibre and a more accurate methodology is a matter for future work. Although the methodology was revealed robust enough in investigating the aerodynamic behaviour of fragments, the images captured for fibres were not qualified for obtaining statistically safe results from automated image analysis. This is because the fibres tended to spread on a larger area with respect to fragments and fewer particles were observed in the light sheet. The shape of the fibre pieces possibly prevents them from falling straight downward, increasing the likelihood of transversal or out-of-plane movements. This highlights the need to release a large number of fibres and to produce more pictures, in order to obtain a more reliable analysis. Furthermore, the release system was not optimal concerning the use of fibres because of the aggregative fluidisation of the material. This makes it difficult to separate single traces, so that the individual behaviour of the fibres gets lost. Although the use of the pressurised air helped to unbind such a structure, the design of the dispenser must be adapted in order to provide reliable results. For these reasons, this work does not supply quantitative results for plastic fibres.

4. Analysis, results and discussion

As regards the analysis of the measurements, the experimental issues mentioned in previous Section 3.3 may result in a number of incorrect traces, biasing the data essentially towards lower settling velocities because of too short particle tracks being recorded. Thus, we had to adopt a filtering approach that can prevent underestimating the actual values of the velocities. Once the raw data were processed, the values of the settling velocities estimated for all samples were compared to reference values used in MPs studies from literature and to values calculated with the Stokes' law and with the general formula of the drag force. The results of the analysis of the experimental data are here reported and discussed.

4.1. Analysis of the measured settling velocities

By assuming a continuous distribution of observed settling velocities, the sampled data was analysed with regard to a consistent and possibly Gaussian distribution of measured velocities. Based on different percentiles of measured values, a threshold settling velocity was defined for identifying outliers and estimating robust and consistent results. The threshold was determined by taking only the rightmost $n\%$ of the distribution of the raw data, i.e. those data that correspond to the highest values for the settling velocity. The data selected for the analysis are those corresponding to a settling velocity $v_s > v_{thr}$, where v_{thr} represents the nth percentile of the raw distribution. Since the choice of the threshold is still arbitrary, we compared six different threshold choices, namely the $n\text{th} = 40\text{th}, 50\text{th}, 60\text{th}, 70\text{th}, 80\text{th}$ and 90th percentile of the distribution of the raw data, respectively.

Fig. 4 shows the histograms of the different MP fragments, PVC, PET and LDPE, for the filtered settling velocities according to two thresholds, $n\text{th} = 60\text{th}, 80\text{th}$ percentiles (histograms for the thresholds $n\text{th} = 70\text{th}, 90\text{th}$ are reported in Figure SM1 of the Supplementary Material). The bin width for the histograms in Fig. 4 was chosen according

Table 2
Statistical parameters of the measured settling velocity distributions for the three samples using different filtering thresholds.

Material	nth percentile Filter	$\langle v_s \rangle$ (ms^{-1})	σ (ms^{-1})	Median (ms^{-1})	Min v_s (ms^{-1})	Max v_s (ms^{-1})
PVC	40	0.05	0.09	0.02	0.002	0.63
	50	0.06	0.11	0.02	0.005	
	60	0.06	0.11	0.02	0.005	
	70	0.08	0.13	0.03	0.009	
	80	0.12	0.15	0.05	0.02	
	90	0.20	0.16	0.14	0.05	
PET	40	0.07	0.11	0.02	0.005	0.79
	50	0.07	0.11	0.02	0.005	
	60	0.08	0.12	0.03	0.007	
	70	0.11	0.13	0.05	0.01	
	80	0.15	0.14	0.1	0.02	
	90	0.24	0.15	0.19	0.09	
LDPE	40	0.06	0.19	0.005	0.001	1.23
	50	0.09	0.23	0.01	0.002	
	60	0.09	0.23	0.01	0.002	
	70	0.14	0.28	0.02	0.005	
	80	0.21	0.33	0.03	0.01	
	90	0.32	0.36	0.08	0.02	

to the Freedman–Diaconis rule (Freedman and Diaconis, 1981) and was calculated as:

$$\Delta = 2\frac{IQR(x)}{n^{1/3}}, \tag{13}$$

where $IQR(x)$ is the interquartile range of the data set x and n is the number of observations. The bin number was calculated as:

$$N = \frac{x_{max} - x_{min}}{\Delta}, \tag{14}$$

where x_{max} and x_{min} are the maximum and minimum values in the data set. N was then rounded up in the case of fractional values. This rule was designed to minimise the integral of the squared difference between the histogram of the set of empirical data and the theoretical probability distribution. It ensures a consistent setting of the bins, so that the histograms reflect the actual behaviour of the velocity distribution while remaining comparable.

In Table 2, the statistics related to the histograms, with the addition of the measures also for the thresholds of nth = 40th, 50th percentiles, are reported. Note that, when creating the histograms of the different distributions, the uncertainty associated with the sensitivity of the rule used to estimate the particle travel distances (see Section 3) is much smaller than the standard deviation of the distribution. Thus, we took the latter value as the uncertainty of the distribution.

As highlighted by the histograms, most of the signal in the distribution is concentrated in the low-velocity range, as confirmed also by the median of the distributions, much closer to the minimum value of velocity than the maximum, as in Table 2. Overall, the average values for the different materials get similar when reducing the threshold, while their difference tends to increase when the threshold criterion becomes more stringent. How to choose the filtering threshold is a matter of discussion yet, since the density and the size of the distributions are different. A possible criterion might be choosing the nth percentile for which the averages of the samples start becoming substantially different. This is because, for a low value of nth, the ratio between the number of data coming from true traces and the number deriving from the false ones, representative of a signal-to-noise ratio, might be too small.

In Fig. 5 the behaviour of the average values of v_s as a function of the percentile is reported for the PVC (red line), PET (blue line) and LDPE (black line). It can be seen that the averages tend to get closer when reducing the threshold, i.e. when increasing the amount of analysed data. This is because the sources of uncertainties act in the same way for all the cases. Thus, a possible criterion for choosing the threshold might be to consider the percentile for which the averages start to separate. On the basis of these considerations, for this specific case, nth = 70th or nth = 80th percentiles seem to be appropriate. For the highest values of the threshold, from nth = 70th to nth = 90th, the samples of PVC and PET have closer values of the average velocity, $\langle v_s \rangle$, and its standard deviation, σ.

Comparing the values in Table 2 for the different materials, the greater similarities between PET and PVC would suggest that the density of the material plays a significant role in determining the settling velocity of the MP particles. However, it is difficult to conclusively disentangle the contribution of the particle size on the velocity value with respect to the density of the material. Even when using selected and controlled samples, the imprecision in the real dimension of the particles may thus be an issue when the intention is to identify the relative contribution of the different parameters characterising the various plastic materials and, consequently, their dynamics in the air.

The choice of the threshold is found to play a crucial role in correctly filtering out most of the false signals generated by the uncertainties of the setup. Therefore the analysis presented in Figs. 4 and 5 can be, at the same time, a simple and proper approach to be applied when repeating the experiments with analogous setups, in order to account for the potential variability of the results.

To verify and confirm the validity of the threshold approach to handle the noise processes, a Fourier analysis was applied. A discrete Fourier series of the velocity distribution can be written as:

$$\mathcal{G}(k) = \frac{1}{N}\sum_{j=0}^{N-1} g(v_j)\exp\left(\frac{2\pi k i v_j}{N}\right) \tag{15}$$

where N is the number of elements in the vector $g(v_j)$, i.e. the sample distribution, $k = 1/v$ is the estimation of the velocity scale associated to each mode, v_j is the jth element of the velocity vector. This decomposition separates the contribution of each velocity bin, providing the weight of the jth element of the velocity into the total spectrum. If the noise process acts as a common background for the three different samples and it is predominant in the low-velocity regime, the three spectra should converge above a given k. Fig. 6a shows the squared module of Fourier spectra normalised to the integral of the spectra as a function of k for positive values of the frequency ($k > 0$). The plotted quantity is:

$$\mathcal{F}(k) = \frac{|\mathcal{G}(k)|^2}{\sum_k |\mathcal{G}(k)|^2} \tag{16}$$

The spectra of PVC and PET are close in the low frequency regime (i.e. high speed) and both differ from the LDPE spectrum, which has a reduced slope when compared to them. Such different trend of the LDPE spectrum can be related to the nature of its sample (Table 1), characterised by a large number of small particles (the size spectrum has a median of 31 μm), so that part of the signal in the velocity spectrum may overlap with the noise. For $k > 60$, PVC and LDPE spectra tend to overlap while the PET one shows a tendency to slightly decrease before reaching an analogous asymptotical behaviour, not converging exactly to the same value. This may happen because some of the noise sources may be affected by the signal itself, e.g. considering the fragmentation of the traces, thus changing the single contribution of each k into the total spectrum.

Given that the spectra reach an asymptotical behaviour, to identify a value of k representative of the noise threshold, at which the saturation of the spectra is expected to occur, we consider the derivatives of the curves, as in Fig. 6b. For low values of k the slope associated with the LDPE sample is almost flat while the derivatives of PVC and PET show a more irregular behaviour. For $k > 40$ the three curves become comparable and tend to flatten. This indicates that the saturation of the spectra is simultaneously reached for $k > 40$, when each Fourier mode contributes in a similar way for the three samples.

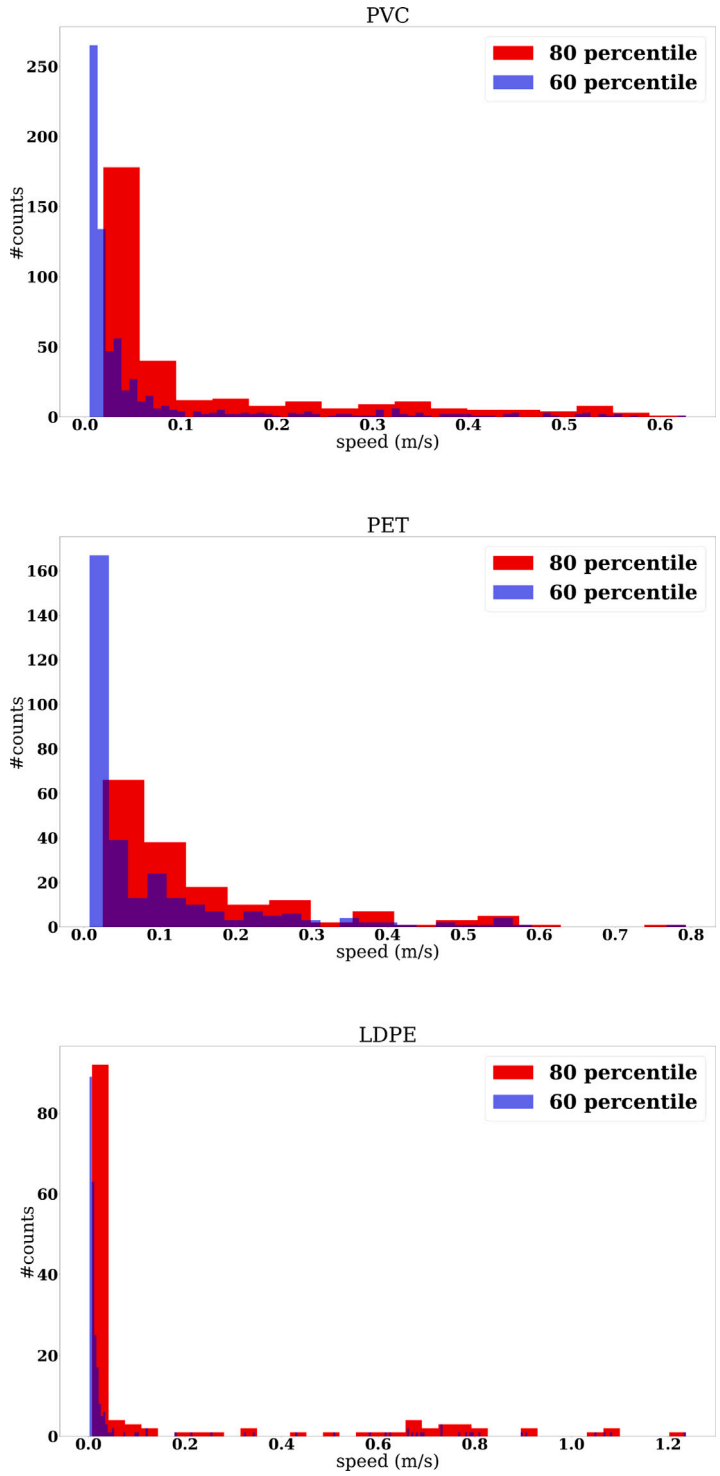

Fig. 4. Histograms of the distribution for the nth = 60th (blue colour) and nth = 80th (red colour) percentile thresholds, for PVC (top panel), PET (central panel) and LDPE (bottom panel) samples. (For interpretation of the references to colour in this figure legend, the reader is referred to the web version of this article.)

It can thus be inferred that a source of the signal at low speed acts in the same way for the three samples. Since the experimental setup is the same, it is reasonable to assume that the saturation of the spectra is mainly associated to noise. For this reason, the value of the velocity corresponding to $k = 40$, that is $v = 0.025$ ms^{-1}, can define a threshold for the actual MPs settling velocity. Looking at the statistics in Table 2, mean, median and minimum values, this analysis confirms that the 80th and 90th percentiles represent a safe threshold to filter out the noise contribution.

4.2. Comparison and evaluation of the settling velocities

To compare the range of the measured settling velocities with theoretical estimates, besides the Stokes' law $F_{d-Stokes} \propto v$, having the limitations discussed in Section 2, we also considered the general formula for the drag force, which reads

$$F_d = \frac{1}{2}\rho_f C_D A v^2 \tag{17}$$

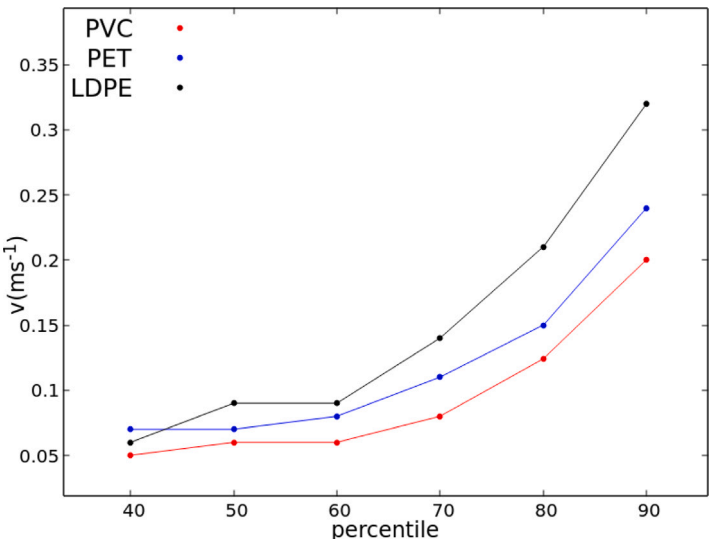

Fig. 5. Behaviour of the average settling velocity $\langle v_s \rangle$ as a function of the nth-percentile threshold for the three plastic samples, PVC (red line), PET (blue line) and LDPE (black line). (For interpretation of the references to colour in this figure legend, the reader is referred to the web version of this article.)

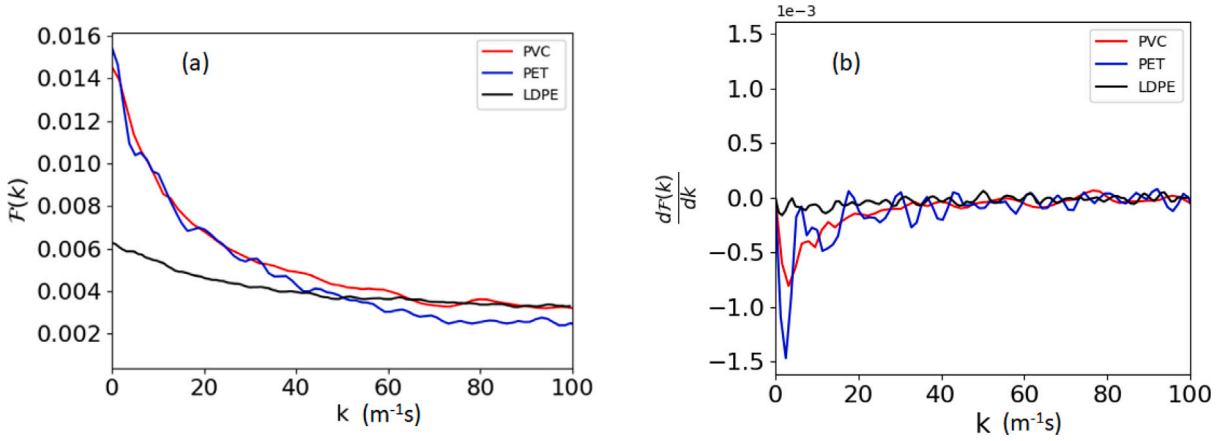

Fig. 6. Plots of the curves of (a) the Fourier spectra and (b) their derivatives, as functions of $k = v^{-1}$, for the PVC (red line), PET (blue line) and LDPE (black line) samples. (For interpretation of the references to colour in this figure legend, the reader is referred to the web version of this article.)

where C_D is the drag coefficient, and A is the frontal area of the object facing the fluid.

In Table 3 the values of the velocity calculated with the Stokes' law (Eq. (2)) and from the balance between the gravitational force and the general drag-force (Eq. (17)), are reported for the nominal size of the particles of the samples and their minimum, mean and maximum sizes estimated by microscope as in Table 1. The values used for the air density and dynamic viscosity correspond to a temperature of 20 °C, thus $\rho_f = 1.204$ kg m^{-3}, $\mu = 1.825\ 10^{-5}$ kg m^{-1}s^{-1}. In the general drag-force formula, we assigned $C_D = 1.2$ ($Re \sim 10^2$) for a spherical particle falling in an almost laminar ($v_{Gen-lam}$) flow, considering that the air in the wind tunnel can never be truly stationary.

The experimental estimates of the settling velocity values referring to the nominal size (see also Table 2), largely differ from those resulting from the Stokes formula applied using the nominal diameter size, as in Table 3. Notice that the Stokes velocity calculated for the mean measured size is of the order of the highest values of the observed settling velocities for PVC and PET. Instead, for LDPE it takes values analogous to the lowest measured ones. This may be related to the previous results of the Fourier analysis, where the velocity spectrum highlighted that part of the signal might overlap with the noise, because of the high number of small particles in the LDPE sample. There is instead a full agreement between the values of the Stokes velocity calculated for the minimum size and the minimum values of the measured velocity referring to the set filtered at the 80th percentile. The maximum measured velocities take values in between those estimated using the general drag-force formula and Stokes' law, but when they are applied to particles of much smaller diameters, as can be seen looking at the values for the minimum and mean sizes. This analysis quantifies the potential limitations of the straight applicability of the Stokes' law for the types of heterogeneous samples, and related particle sizes, considered in this study, as discussed in Section 2. Given that in the real field the MP samples are actually heterogeneous, the Stokes' law should be cautiously applied. As for the general drag-force formula, notice that the frontal area will constantly change for non-spherical particles, making drag forces non-stationary and perhaps maximising or minimising the bulk settling velocity of an ensemble of different particles. Thus, also its applicability to calculate settling velocities of real MPs should be carefully considered.

As an exercise, we computed the length of the diameter in Stokes' law that a particle should have to get the averaged observed values of the settling velocity. In Table 4 the results are reported considering all raw data and the 40th and 90th percentile filtering thresholds. As predictable, the equivalent diameters foreseen by the Stokes' law take values about an order of magnitude smaller than the nominal sizes reported in Table 1. This indicates a substantially larger drag of

Table 3
Values of the measured settling velocities for the three samples, compared to values calculated with the Stokes' law and with the general drag-force laws, referring to the particle sizes in Table 1.

Material	Min v_s (ms^{-1}) 80th perc filter	Max v_s (ms^{-1})	Size	d (μm)	v_{Stokes} (ms^{-1})	$v_{Gen-lam}$ (ms^{-1}) $C_D = 1.2$
PVC	0.02	0.63	nominal	250	2.61	1.78
			min	20	0.02	0.50
			mean	125	0.65	1.26
			max	297	3.68	1.94
PET	0.02	0.79	nominal	300	3.71	1.94
			min	21	0.02	0.51
			mean	95	0.37	1.09
			max	290	3.46	1.90
LDPE	0.01	1.23	nominal	300	2.47	1.58
			min	19	0.01	0.40
			mean	41	0.05	0.58
			max	271	2.02	1.50

Table 4
Size of the equivalent particle's diameters calculated with the Stokes' law when using the observed values of the settling velocity in it.

Material	nth-percentile Filter	Measured $\langle v_s \rangle$ (ms^{-1})	Equivalent Stokes diameter (μm)
PVC	all data	0.04	31
	40	0.05	35
	90	0.20	69
PET	all data	0.04	31
	40	0.07	41
	90	0.24	76
LDPE	all data	0.06	38
	40	0.06	38
	90	0.32	88

the tested particles than an ideal sphere would generate. The reasons could be either a different flow regime around the particle or, more likely, a strong effect of the expected rotation/tumbling/movement of irregularly shaped particles in the flow.

Notice that when referring only to the nominal size of the different materials, the ratio K between the measured velocity $\langle v_s \rangle$ for the 80th percentile and the velocity v_{Stokes} that would be estimated with Stokes' law, takes values $K = 0.048,\ 0.04,\ 0.085$ for PVC, PET and LDPE. Looking at the parameters in Table 1, the similar K values for PVC and PET would again suggest that the density of the material may play a substantial role besides the (nominal) size of the particles. However, when referring to the mean measured sizes, 125 μm for PVC and 95 μm for PET (Table 3), the ratios are $K = 0.18,\ 0.40$ respectively, thus such consideration remains not conclusively confirmed.

The values of the settling velocity measured in the BURNIA experiments $\langle v_s \rangle$, are compared in Table 5 to those calculated by Wright et al. (2020), v_{s-Wr}, and by Trainic et al. (2020), v_{s-Tr}, for MP fragments. The v_{s-Wr} value is larger than v_{s-Tr} and characterises particles of analogous size but higher density. For BURNIA velocities, we included the values for both the 80th and 90th percentile filters, since they are representative of the largest particles, thus approaching the nominal sizes. BURNIA PVC and PET have both a higher density and a larger nominal size than the particles in Wright et al. (2020) and Trainic et al. (2020). Their $\langle v_s \rangle$ values are more similar to v_{s-Tr}, denoting an analogous balance between gravitational and drag forces that are both larger. The range of LDPE $\langle v_s \rangle$ values lies between v_{s-Tr} and v_{s-Wr}, for particles having similar densities but one-third of the LDPE nominal size. In this case, the analogy seems to be connected to the density, yet the LDPE sample showed a large variability in the particle sizes. Thus, this consideration has to be retained *cum grano salis*, given the uncertainties linked to the measuring approach and considering the heterogeneity of the MPs in the samples, even when proper filtering is applied to the raw data.

Since our measured values are in the order of those reported in the literature, we may consider them reasonable, despite the uncertainties previously discussed. For reference, the results presented in Khvorostyanov and Curry (2002) Fig. 2 for water drops of diameter $\lesssim$ 500 μm falling in standard atmosphere, show values for the settling velocity within 0.2 ms^{-1}, supporting the range of values observed in our experiments.

5. Conclusion and future work

The settling velocity is one of the essential parameters that determine the airborne lifetime of MPs in the atmosphere, thus the scale of their potential transport. It represents also an important input for the application of the atmospheric dispersion models, since gravitational sedimentation substantially contributes to the deposition processes. Providing a proper estimate of the settling velocity for MP fragments and fibres is thus crucial to properly simulate their transport at short and long distances. In particular, when dealing with the detection of MPs in remote and pristine regions it is important to quantify the effectiveness of deposition, which influences the potential of long-range transport (Martina and Trini Castelli, 2023). Reliable estimates for settling velocities may be decisive for reconstructing airborne transport pathways, source areas and related time scales.

Here we investigated the feasibility of measuring the settling velocities of different plastic micro-particles in a controlled laboratory experiment, in wind tunnel facilities. The experimental configuration allows for both, measuring effective settling velocities of particles in calm air as well as for measuring effective deposition velocities in turbulent flows. An initial and simple experimental setup, named BURNIA, was developed paying attention to reproducing an undisturbed fall of the particles in calm air. The MP samples were made of PVC, PET and LDPE particles of nominal size of ≃250–300 μm, which correspond to plastic fragments, and fibres were also tentatively used. A microscope analysis of the plastic particles in the samples enabled highlighting the heterogeneity of their dimension, despite the nominal values indicated by the supplier. Such variability was accounted for when calculating the correspondent settling velocities using theoretical formulas.

One of the aims was to present the approach that we propose to elaborate and analyse the observed data. We discussed the advantages and disadvantages of the methodology, as well as an analysis of the sources of noise and uncertainty. Addressing the uncertainty of measurements and results is one of the most challenging problems that we encountered during these exploratory experiments, and its correct handling is crucial in order to retrieve reliable results. The effect of different levels of filtering for the raw data was assessed with reference to their distributions. The analysis suggested retaining data which lie above the 70th percentile of the observed velocity values to exclude potentially erroneous data from further analysis. Based on the statistical analysis applied to the measurements performed during several experiments in the wind tunnel, the mean values of the settling velocities

Table 5
Comparison of the BURNIA observed settling velocity $\langle v_s \rangle$ values, filtered with the 80th and 90th percentiles, with values estimated by Wright et al. (2020) and Trainic et al. (2020).

Set and material	Density ρ_p (kgm^{-3})	Size d or l (μm)	Settling velocity v_s (ms^{-1})
BURNIA PVC	1400	250	0.12–0.20
BURNIA PET	1380	300	0.15–0.24
BURNIA LDPE	920	300	0.21–0.32
Wright et al. (2020) PS	1050	100	0.32
Trainic et al. (2020) PE	940	102 × 97	0.20

were found to range between 0.1 and 0.2 ms^{-1}, when referring to the 80th percentile filter. These values are similar to those used in the literature studying the airborne MPs. A Fourier analysis of the observations indicated a threshold minimum value of 0.025 ms^{-1} to be adopted for filtering the noise out of the data. Challenges were then reviewed and possible improvements of the test configuration were pondered, like focusing on smaller particle sizes, dealing properly with fibrous MP type and quantifying the effective settling velocity of MPs in turbulent wind conditions. The related discussion was aimed at enabling the reproducibility of the experiments in other laboratories.

Considering that the size of the plastic particles used in the experiments lies in the range of definition for the MPs, we discussed the applicability of the Stokes' law, used in many studies also for MPs, for determining the settling velocities. An initial bias could have been the dimension of the particles in the available samples, since the Stokes' law is defined for spherical particles and found applicable for diameters in the range 1–80 μm. Previous studies applied it to MPs particles of sizes from 25 μm to 50 μm (Allen et al., 2019), and 100 μm (Wright et al., 2020), therefore they were less confronted with that limitation in the applicability of Stokes' law. Yet, the analysis of the size spectrum of the samples available to us showed that they contained particles with rather different sizes. In any case, applying the Stokes' law for the MPs used in our experiments generally led to an overestimation of the settling velocities. It is also important to recall that the atmosphere itself is intrinsically turbulent, thus the assumption of very small Reynolds numbers and a viscous flow correspond to a condition that can hardly be met. In this sense, the use of the Stokes' law to assess and estimate the MP settling velocity in the air should be more thoroughly tackled. Recent works carried out related investigations, which can be of reference for future developments of our approach too. Goral et al. (2023) measured settling velocities in analogous ranges of values as our estimates, for MP particles of different densities and shapes falling in distilled water. They also proposed empirical formulations to correct the drag coefficients for each particle shape. Preston et al. (2023) measured settling velocities for MPs characterised by varied densities and four idealised shapes – spheres, cylinders, fibres and films – performing release experiments into an isolated fall column. They assessed the implications of the MPs shape, size and aerodynamic characteristics on modelling their atmospheric transport, highlighting that applying Stokes' law in numerical models leads to a substantial overestimation of the MPs settling velocity values. However, in our experiments we are treating the settling of an ensemble of heterogeneous particles in the air, an intrinsically turbulent medium also in indoor environments. These aspects present additional challenges than considering flows that can be stationary and still. We also note that when dealing with the real atmosphere, other forces act on a particle, driven by wind, radiative processes and convection, pressure fluctuations and turbulence. Thus it is demanding to move to the more general concept of 'deposition velocity', which is more representative of the effective time particles may spend in the air.

This contribution was aimed at shedding light on the issue of properly estimating the settling velocity of MP particles in the air and related complexities. Further investigations are planned based on wind-tunnel experiments, and additional physical processes like resuspension and grass-hopper effect will be studied in future phases to achieve a better understanding of the specific MP dynamics in the atmosphere.

Funding information

This research did not receive any specific grant from funding agencies in the public, commercial, or not-for-profit sectors.

CRediT authorship contribution statement

Matteo M. Musso: Writing – review & editing, Writing – original draft, Visualization, Software, Methodology, Investigation, Formal analysis, Data curation. **Frank Harms:** Visualization, Validation, Methodology, Investigation, Formal analysis, Data curation. **Massimo Martina:** Software, Methodology, Investigation, Formal analysis, Data curation. **Elke K. Fischer:** Writing – review & editing, Resources, Methodology, Investigation, Conceptualization. **Bernd Leitl:** Writing – review & editing, Writing – original draft, Supervision, Resources, Methodology, Investigation, Conceptualization. **Silvia Trini Castelli:** Writing – review & editing, Writing – original draft, Supervision, Resources, Methodology, Investigation, Conceptualization.

Declaration of competing interest

The authors declare that they have no known competing financial interests or personal relationships that could have appeared to influence the work reported in this paper.

Data availability

Data will be made available on request.

Appendix A. Supplementary data

Supplementary material related to this article can be found online at https://doi.org/10.1016/j.hazadv.2024.100433.

References

Allen, D., Allen, S., Abbasi, S., Baker, A., Bergmann, M., Brahney, J., Butler, T., Duce, R.A., Eckhardt, S., Evangeliou, N., Jickells, T., Kanakidou, M., Kershaw, P., Laj, P., Levermore, J., Li, D., Liss, P., Liu, K., Mahowald, N., Masque, P., Materic, D., Mayes, A.G., McGinnity, P., Osvath, I., Prather, K.A., Prospero, J.M., Revell, L.E., Sander, S.G., Shim, W.J., Slade, J., Stein, A., Tarasova, O., Wright, S., 2022. Microplastics and nanoplastics in the marine-atmosphere environment. Nat. Rev. Earth Environ. 3, 393–405. http://dx.doi.org/10.1038/s43017-022-00292-x.

Allen, S., Allen, D., Moss, K., Le Roux, G., Phoenix, V.R., Sonke, J.E., 2020. Examination of the ocean as a source for atmospheric microplastics. Plos One 15. http://dx.doi.org/10.1371/journal.pone.0232746.

Allen, S., Allen, D., Phoenix, V.R., Le Roux, G., Jimenez, P.D., Simonneau, A., Binet, S., Galop, D., 2019. Atmospheric transport and deposition of microplastics in a remote mountain catchment. Nat. Geosci. 12, http://dx.doi.org/10.1038/s41561-019-0335-5, 339+.

Ambrosini, R., Azzoni, R.S., Pittino, F., Diolaiuti, G., Franzetti, A., Parolini, M., 2019. First evidence of microplastic contamination in the supraglacial debris of an Alpine glacier. Environ. Pollut. 253, 297–301. http://dx.doi.org/10.1016/j.envpol.2019.07.005.

Andrady, A.L., 2011. Microplastics in the marine environment. Mar. Pollut. Bull. 62, 1596–1605. http://dx.doi.org/10.1016/j.marpolbul.2011.05.030.

Arthur, C., Baker, J., Bamford, H. (Eds.), 2009. Proceedings of the International Research Workshop on the Occurrence, Effects, and Fate of Microplastic Marine Debris. URL: https://marinedebris.noaa.gov/sites/default/files/publications-files/TM_NOS-ORR_30.pdf.

Aves, A.R., Revell, L.E., Gaw, S., Ruffell, H., Schuddeboom, A., Wotherspoon, N.E., LaRue, M., McDonald, A.J., 2022. First evidence of microplastics in Antarctic snow. Cryosphere 16, 2127–2145. http://dx.doi.org/10.5194/tc-16-2127-2022.

Baba, J., Komar, P.D., 1981. Measurements and analysis of setting velocities of natural quartz sand grains. J. Sediment. Res. 51, 631–640.

Bergmann, M., Collard, F., Fabres, J., Gabrielsen, G.W., Provencher, J.F., Rochman, C.M., van Sebille, E., Tekman, M.B., 2022. Plastic pollution in the Arctic. Nat. Rev. Earth Environ. 3, 323–337. http://dx.doi.org/10.1038/s43017-022-00279-8.

Bradski, G., 2000. The OpenCV Library. Dr. Dobb's J. Softw. Tools.

Brahney, J., Hallerud, M., Heim, E., Hahnenberger, M., Sukumaran, S., 2020. Plastic rain in protected areas of the United States. Science 368, 1257–1260. http://dx.doi.org/10.1126/science.aaz5819.

Bullard, J.E., Ockelford, A., O'Brien, P., Neuman, C.M., 2021. Preferential transport of microplastics by wind. Atmos. Environ. 245. http://dx.doi.org/10.1016/j.atmosenv.2020.118038.

Burns, E.E., Boxall, A.B.A., 2018. Microplastics in the aquatic environment: Evidence for or against adverse impacts and major knowledge gaps. Environ. Toxicol. Chem. 37, 2776–2796. http://dx.doi.org/10.1002/etc.4268.

Cai, L., Wang, J., Peng, J., Tan, Z., Zhan, Z., Tan, X., Chen, Q., 2017. Characteristic of microplastics in the atmospheric fallout from Dongguan city, China: preliminary research and first evidence. Environ. Sci. Pollut. Res. 24, 24928–24935. http://dx.doi.org/10.1007/s11356-017-0116-x.

Dietrich, W.E., 1982. Settling velocity of natural particles. Water Resour. Res. 18, 1615–1626. http://dx.doi.org/10.1029/WR018i006p01615.

Freedman, D., Diaconis, P., 1981. On the histogram as a density estimator: L 2 theory. Z. Wahrscheinlichkeitstheor. verwandte Geb. 57, 453–476.

Goral, K.D., Guler, H.G., Larsen, B.E., Carstensen, S., Christensen, E.D., Kerpen, N.B., Schlurmann, T., Fuhrman, D.R., 2023. Settling velocity of microplastic particles having regular and irregular shapes. Environ. Res. 228. http://dx.doi.org/10.1016/j.envres.2023.115783.

Hartmann, N.B., Hüffer, T., Thompson, R.C., Hassellöv, M., Verschoor, A., Daugaard, A.E., Rist, S., Karlsson, T., Brennholt, N., Cole, M., Herrling, M.P., Hess, M.C., Ivleva, N.P., Lusher, A.L., Wagner, M., 2019. Are we speaking the same language? Recommendations for a definition and categorization framework for plastic debris. Environ. Sci. Technol. 53, 1039–1047. http://dx.doi.org/10.1021/acs.est.8b05297.

Henn, A.R., 1996. Calculation of the Stokes and aerodynamic equivalent diameters of a short reinforcing fiber. Part. Part. Syst. Charact. 13, 249–253.

ISO/TR 21960:2020, 2020. CEN ISO/TR 21960:2021-02. Plastics - Environmental Aspects - State of Knowledge and Methodologies (ISO/TR 21960:2020). Technical Report, CEN ISO, URL: https://www.iso.org/st{anda}rd/72300.html.

Janke, N., 1966. Effect of shape upon the settling vellocity of regular convex geometric particles. J. Sediment. Res. 36, 370–376.

Khvorostyanov, V., Curry, J., 2002. Terminal velocities of droplets and crystals: Power laws with continuous parameters over the size spectrum. J. Atmos. Sci. 59, 1872–1884. http://dx.doi.org/10.1175/1520-0469(2002)059<1872:TVODAC>2.0.CO;2.

Klein, M., Bechtel, B., Brecht, T., Fischer, E.K., 2023. Spatial distribution of atmospheric microplastics in bulk-deposition of urban and rural environments - A one-year follow-up study in northern Germany. Sci. Total Environ. 901. http://dx.doi.org/10.1016/j.scitotenv.2023.165923.

Li, Y., Shao, L., Wang, W., Zhang, M., Feng, X., Li, W., Zhang, D., 2020. Airborne fiber particles: Types, size and concentration observed in Beijing. Sci. Total Environ. 705, 135967. http://dx.doi.org/10.1016/j.scitotenv.2019.135967.

Liu, K., Wu, T., Wang, X., Song, Z., Zong, C., Wei, N., Li, D., 2019. Consistent transport of terrestrial microplastics to the ocean through atmosphere. Environ. Sci. Technol. 53, 10612–10619. http://dx.doi.org/10.1021/acs.est.9b03427.

Martina, M., Trini Castelli, S., 2023. Modelling the potential long-range dispersion of atmospheric microplastics reaching a remote site. Atmos. Environ. 312, 120044. http://dx.doi.org/10.1016/j.atmosenv.2023.120044.

McNown, J.S., Malaika, J., 1950. Effects of particle shape on settling velocity at low Reynolds numbers. EOS Trans. Am. Geophys. Union 31, 74–82.

O'Brien, S., Rauert, C., Ribeiro, F., Okoffo, E.D., Burrows, S.D., O'Brien, J.W., Wang, X., Wright, S.L., Thomas, V.K., 2023. There's something in the air: A review of sources, prevalence and behaviour of microplastics in the atmosphere. Sci. Total Environ. 874. http://dx.doi.org/10.1016/j.scitotenv.2023.162193.

Parolini, M., Antonioli, D., Borgogno, F., Gibellino, M.C., Fresta, J., Albonico, C., De Felice, B., Canuto, S., Concedi, D., Romani, A., et al., 2021. Microplastic contamination in snow from Western Italian Alps. Int. J. Environ. Res. Public Health 18 (768).

Phuong, N.N., Zalouk-Vergnoux, A., Poirier, L., Kamari, A., Châtel, A., Mouneyrac, C., Lagarde, F., 2016. Is there any consistency between the microplastics found in the field and those used in laboratory experiments? Environ. Pollut. 211, 111–123. http://dx.doi.org/10.1016/j.envpol.2015.12.035.

Preston, C.A.A., Neuman, C.L.M.L., Aherne, J., 2023. Effects of shape and size on microplastic atmospheric settling velocity. Environ. Sci. Technol. 57, 11937–11947. http://dx.doi.org/10.1021/acs.est.3c03671.

Rezaei, M., Riksen, M.J., Sirjani, E., Sameni, A., Geissen, V., 2019. Wind erosion as a driver for transport of light density microplastics. Sci. Total Environ. 669, 273–281. http://dx.doi.org/10.1016/j.scitotenv.2019.02.382.

Rochman, C.M., 2018. Microplastics research—from sink to source. Science 360, 28–29. http://dx.doi.org/10.1126/science.aar7734.

Rosato, D.V., Rosato, D.V., Rosato, M.v., 2004. Plastic Product Material and Process Selection Handbook. Elsevier.

Schmidt, C., Krauth, T., Wagner, S., 2017. Export of Plastic Debris by Rivers into the Sea. Environ. Sci. Technol. 51, 12246–12253. http://dx.doi.org/10.1021/acs.est.7b02368.

Trainic, M., Flores, J.M., Pinkas, I., Pedrotti, M.L., Lombard, F., Bourdin, G., Gorsky, G., Boss, E., Rudich, Y., Vardi, A., Koren, I., 2020. Airborne microplastic particles detected in the remote marine atmosphere. Commun. Earth Environ. 1. http://dx.doi.org/10.1038/s43247-020-00061-y.

Wang, X., Li, C., Liu, K., Zhu, L., Song, Z., Li, D., 2020. Atmospheric microplastic over the south China sea and east Indian Ocean: abundance, distribution and source. J. Hazard. Mater. 389. http://dx.doi.org/10.1016/j.jhazmat.2019.121846.

Westbrook, C., 2008. The fall speeds of sub-100μm ice crystals. Q. J. R. Meteorol. Soc. 134, 1243–1251. http://dx.doi.org/10.1002/qj.290.

Wright, S.L., Ulke, J., Font, A., Chan, K.L.A., Kelly, F.J., 2020. Atmospheric microplastic deposition in an urban environment and an evaluation of transport. Environ. Int. 136. http://dx.doi.org/10.1016/j.envint.2019.105411.

Xu, C., Zhang, B., Gu, C., Shen, C., Yin, S., Aamir, M., Li, F., 2020. Are we underestimating the sources of microplastic pollution in terrestrial environment? J. Hazard. Mater. 400, 123228. http://dx.doi.org/10.1016/j.jhazmat.2020.123228.

Zender, C.S., Bian, H., Newman, D., 2003. Mineral Dust Entrainment and Deposition (DEAD) model: Description and 1990s dust climatology. J. Geophys. Res.: Atmos. 108.

Zhang, Y., Gao, T., Kang, S., Allen, S., Luo, X., Allen, D., 2021. Microplastics in glaciers of the Tibetan Plateau: Evidence for the long-range transport of microplastics. Sci. Total Environ. 758, 143634. http://dx.doi.org/10.1016/j.scitotenv.2020.143634.

Zhang, Y., Kang, S., Allen, S., Allen, D., Gao, T., Sillanpaa, M., 2020. Atmospheric microplastics: A review on current status and perspectives. Earth-Sci. Rev. 203. http://dx.doi.org/10.1016/j.earscirev.2020.103118.